BIOCHEMISTRY
including biophysical chemistry & molecular biology
Article

Biochemistry **2010,** *49,* 6737–6745 6737
DOI: 10.1021/bi100912m

Structure of the Human Sulfhydryl Oxidase Augmenter of Liver Regeneration and Characterization of a Human Mutation Causing an Autosomal Recessive Myopathy[†,‡]

Vidyadhar N. Daithankar, Stephanie A. Schaefer, Ming Dong, Brian J. Bahnson,* and Colin Thorpe*

Department of Chemistry and Biochemistry, University of Delaware, Newark, Delaware 19716

Received June 7, 2010; Revised Manuscript Received June 28, 2010

ABSTRACT: The sulfhydryl oxidase augmenter of liver regeneration (ALR) binds FAD in a helix-rich domain that presents a CxxC disulfide proximal to the isoalloxazine ring of the flavin. Head-to-tail interchain disulfide bonds link subunits within the homodimer of both the short, cytokine-like, form of ALR (sfALR), and a longer form (lfALR) which resides in the mitochondrial intermembrane space (IMS). lfALR has an 80-residue N-terminal extension with an additional CxxC motif required for the reoxidation of reduced Mia40 during oxidative protein folding within the IMS. Recently, Di Fonzo et al. [Di Fonzo, A., Ronchi, D., Lodi, T., Fassone, E., Tigano, M., Lamperti, C., Corti, S., Bordoni, A., Fortunato, F., Nizzardo, M., Napoli, L., Donadoni, C., Salani, S., Saladino, F., Moggio, M., Bresolin, N., Ferrero, I., and Comi, G. P. (2009) *Am. J. Hum. Genet. 84*, 594−604] described an R194H mutation of human ALR that led to cataract, progressive muscle hypotonia, and hearing loss in three children. The current work presents a structural and enzymological characterization of the human R194H mutant in lf- and sfALR. A crystal structure of human sfALR was determined by molecular replacement using the rat sfALR structure. R194 is located at the subunit interface of sfALR, close to the intersubunit disulfide bridges. The R194 guanidino moiety participates in three H-bonds: two main-chain carbonyl oxygen atoms (from R194 itself and from C95 of the intersubunit disulfide of the other protomer) and with the 2′-OH of the FAD ribose. The R194H mutation has minimal effect on the enzyme activity using model and physiological substrates of short and long ALR forms. However, the mutation adversely affects the stability of both ALR forms: e.g., by decreasing the melting temperature by about 10 °C, by increasing the rate of dissociation of FAD from the holoenzyme by about 45-fold, and by strongly enhancing the susceptibility of sfALR to partial proteolysis and to reduction of its intersubunit disulfide bridges by glutathione. Finally, a comparison of the TROSY-HSQC 2D NMR spectra of wild-type sfALR and its R194H mutant reveals a significant increase in conformational flexibility in the mutant protein. In sum, these in vitro data document the major impact of the seemingly conservative R194H mutation on the stability of dimeric ALR and complement the in vivo observations of Di Fonzo et al.

Augmenter of liver regeneration (ALR;[1] also abbreviated as GFER, HPO, and HSS) is a representative of a group of small sulfhydryl oxidases whose founding member, Erv1p, was first recognized as a protein essential for respiration and vegetative growth in yeast (*1*, *2*). Since that time a number of Erv/ALR family members have been characterized including yeast Erv2p and ALR analogues from certain double-stranded DNA viruses and from plants and animals (*3*). These proteins share a common flavin binding fold in which the isoalloxazine ring is inserted into the mouth of a bundle of four helices (*3*). This novel flavin binding mode, first recognized for yeast Erv2p (*4*) and then for rat ALR (*5*) and yeast Ero1p (*6*), is found in all of the well-characterized sulfhydryl oxidases including the larger multi-domain quiescin-sulfhydryl oxidase (QSOX) enzymes (*7*−*10*).

Mammalian ALR is a covalent homodimer and is found in two splice variants (*11*−*16*). The short form (sfALR, 15 kDa, starting at M81 of the human long form, lfALR, sequence depicted in Figure 1A) is a circulating growth factor (*11*, *12*, *15*, *17*, *18*) and interacts with specific receptors on the cell surface (*19*, *20*). Receptors for sfALR stimulate the mitogen-activated protein kinase cascade leading to enhanced liver regeneration (*19*, *21*) and recovery of renal tubular cells from ischemic/reperfusion injury (*22*). sfALR is also found in the cytosol and in the nucleus and interacts with Bcl-2/adenovirus E1B 19 kDa interacting protein 2-like (*23*) that confers protection against the effects of viral infection and proapoptotic stimuli (*24*). sfALR also binds to Jun activation domain-binding protein 1 of the mammalian COP9 signalosome (*25*). While interest in sfALR is increasing, specific details concerning its enzymatic activity, locale, and mode of action remain unclear.

[†]This work was supported in part by National Institutes of Health Grant GM26643 (C.T.), 2P20RR015588 from the National Center for Research Resources (B.J.B.), and USPHS Training Grant 1-T32-GM08550 (S.A.S.). The content of this work is solely the responsibility of the authors and does not necessarily reflect the official views of the National Institute of General Medical Sciences or the National Institutes of Health.

[‡]Protein Data Bank entry code 3MBG represents the atomic coordinates and structure factors for the short form of human augmenter of liver regeneration.

*Authors for correspondence. B.J.B.: phone, 302-831-0786; fax, 302-831-6335; e-mail, bahnson@udel.edu. C.T.: phone, 302-831-2689; fax, 302-831-6335; e-mail, cthorpe@udel.edu.

[1]Abbreviations: ALR, augmenter of liver regeneration (lfALR and sfALR refer to long and short forms of the protein, respectively); DTNB, 5,5′-dithiobis(2-nitrobenzoate); DTT, dithiothreitol; GSH, reduced glutathione; GSSG, oxidized glutathione; TROSY, transverse relaxation optimized spectroscopy; HSQC, ^{15}N heteronuclear single-quantum coherence; IMS, mitochondrial intermembrane space; IPTG, isopropyl D-thiogalactopyranoside; NEM, *N*-ethylmaleimide; QSOX, quiescin-sulfhydryl oxidase; rmsd, root-mean-square deviation.

Published on Web 07/01/2010

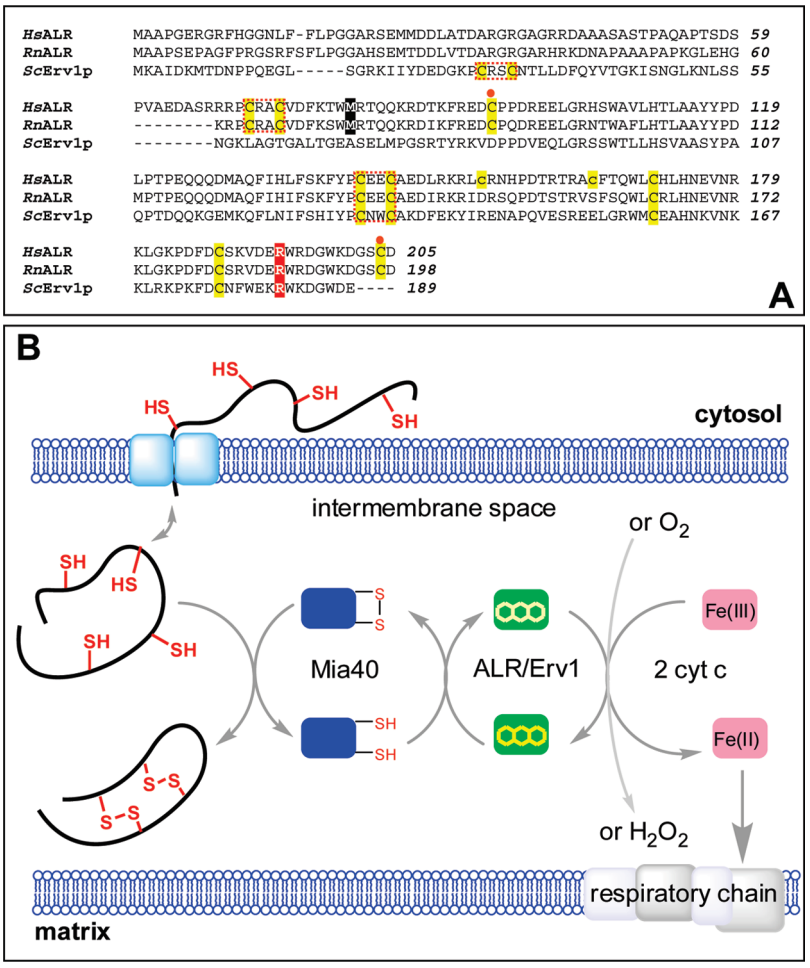

FIGURE 1: Comparison of sequences of human and rat ALR with yeast Erv1p and a depiction of the role of ALR in oxidative folding in the mitochondrial intermembrane space. Human, rat, and yeast sequences are indicated by *Hs*, *Rn*, and *Sc* prefixes, respectively, in the alignment shown in panel A. All cysteines are highlighted in yellow. The N-terminal (distal) and C-terminal (proximal) redox-active CxxC motifs are enclosed within red dotted boxes. The cysteine residues forming intersubunit disulfide bonds are denoted by orange circles. The two cysteine residues in human ALR that are mutated to prevent aggregation are shown in lower case. The methionine residue highlighted in black represents the N-terminus of the short form of mammalian ALR. The position of the R194 mutant in human ALR is highlighted in red. Panel B: Proteins undergoing oxidative folding in the IMS transfer electrons to Mia40 which then transmits them to long form ALR (or Erv1p in yeast). The terminal electron acceptor is either cytochrome *c* or molecular oxygen.

Long-form ALR (23 kDa), like its yeast counterpart, Erv1p, populates the intermembrane space (IMS) of the mitochondrion, where it participates in a chain of disulfide exchange reactions that generate disulfide bonds in a number of resident proteins with twin Cx_3C and Cx_9C motifs (*26*−*37*) (Figure 1B). ALR is currently classified as a flavoprotein oxidase catalyzing the generation of disulfides with the stoichiometry:

$$2R-SH + O_2 \rightarrow R-S-S-R + H_2O_2$$

However, cytochrome *c* is a much better electron acceptor than oxygen for both sf- and lfALR in vitro (*38*, *39*). This finding led us to suggest that reduction of cytochrome *c* could minimize the generation of reactive oxygen species associated with generation of disulfides in the IMS (Figure 1B (*38*)). Subsequent in vivo studies of the yeast mitochondrial IMS have confirmed that Erv1p and cytochrome *c* can interact productively during oxidative folding (*37*, *40*). Alternatively, any hydrogen peroxide liberated from these flavoprotein sulfhydryl oxidases could reoxidize cytochrome *c* catalyzed by cytochrome *c* peroxidase within the IMS (*41*).

In an interesting recent communication, Comi and colleagues (*42*) describe the first human ALR mutation to be recognized. Three children from consanguineous parents developed cataract, progressive muscle hypotonia with developmental delay, and hearing loss. Di Fonzo et al. identified the missense mutation which results in the substitution of an arginine for a histidine at position 194 (*42*). While this R194H mutation did not affect the levels of mRNA, it appeared to impact the import and/or stability of the mutant protein in the mitochondrial IMS. Primary myoblasts from an affected sibling showed an approximately 2-fold increase in doubling time, again consistent with a significant impact of the mutant on cell function (*42*). Di Fonzo et al. further sought to characterize the mutant by generating the analogous mutation (R182H) in yeast Erv1p. In this background, the mutation significantly impacted cytochrome oxidase biosynthesis because Erv1p is involved in the folding of the copper chaperones required for metal insertion into this respiratory chain component (*43*). However, the focus of their study was neither an enzymological characterization of the human mutant nor a discussion of the molecular environment of R194 and the interactions it might make with neighboring residues.

Herein we characterize the R194H mutation in the context of our continuing enzymological studies of human ALR (*38*, *39*, *44*). While the yeast Erv1p analogue of ALR proved a useful starting

point for evaluation of the behavior of the R194H mutation (*42*), there are significant differences between the yeast and mammalian orthologues. For example, the distal CxxC disulfide responsible for shuttling reducing equivalents from Mia40 to the proximal disulfide that is in redox communication with the flavin is placed some 40 residues distant in the primary structure of the two proteins (Figure 1A) (*3*, *39*, *45*). Further, an initial examination of the location of R194 using the published structure of rat ALR (PDB: 1OQC (*5*)) suggests that it is placed close to an interchain disulfide bond in the mammalian proteins and is involved in H-bonding interactions across the subunit interface (see later). Not only does Erv1p lack these interchain disulfides, but there are further significant differences between the sequences of yeast and mammalian orthologues in the vicinity of R194 (Figure 1A). It is therefore important to assess the impact of the R194H mutation with the cognate human protein.

Since a structure of human ALR was unavailable, we have determined a high-resolution crystal structure of the short-form ALR, intending to pair this with a companion structure of the R194H mutant. Although we have been unsuccessful in obtaining crystals of the R194H mutant, we have utilized 2D NMR methods to document a marked increase in protein mobility compared to the corresponding wild-type protein. While the mutant flavoprotein remains fully active in a variety of assays, the resulting protein appears to be less stable, prone to loss of FAD cofactor, susceptible to reduction of its intersubunit disulfide bonds, and sensitive to partial proteolysis. Our findings suggest that R194 is an important participant in a web of molecular interactions that link the binding of flavin to the stability of the intersubunit disulfide bonds. These results support the observations of Di Fonzo et al. (*42*) that the pathology of this ALR mutant reflects, in part, the stability of the protein in vivo.

EXPERIMENTAL PROCEDURES

Materials. Reagents were obtained as described previously (*39*). Polyethylene glycol 8000 was from Thermo Fisher. Zinc acetate was from Allied Chemical and sodium cacodylate from SPI-Chemical.

Mutation, Expression, and Purification of ALR and Arg194 Mutants. The numbering of amino acid residues for sfALR followed that of lfALR. The full sequence of the His-tagged constructs of lf- and sfALR is shown in Figure S1, Supporting Information. Primers for site-directed mutagenesis (obtained from IDT) are listed in Supporting Information. Mutagenesis was performed as described previously (*38*, *39*) and confirmed by sequence analysis (Genewiz Inc.). As before, the two nonconserved and nonessential cysteines (C154 and C165) were mutated to alanine residues to avoid pronounced oxidative aggregation that was encountered in the early stages of work on human ALR (*38*). While two earlier papers (*38*, *39*) designated these double mutants as ALR′, we adopt the simpler abbreviation "ALR" here and refer to the former C154A/C165A protein as "wild type".

The Mia40 construct used in this work had a shorter N-terminal His tag/linker than used in the earlier work (*39*). The amino acid sequence of this shorter construct is shown in Supporting Information (Figure S1). Expression and purification of Mia40, lfALR, and the corresponding R194H mutant followed the procedures described earlier (*39*). Similarly, wild-type and mutant forms of sfALR were obtained as outlined previously (*38*), except that riboflavin was not added to the culture media, and the protease inhibitor cocktail tablets were replaced with 1 mM PMSF, and 1 μM leupeptin. Expression of ^{15}N-labeled human sfALR (using $^{15}NH_4Cl$, 99%; Cambridge Isotope Laboratories) followed the protocol of Marley et al. (*46*).

UV−Vis Spectra. Where necessary, spectra of lf- and sfALR and their R194 mutants were corrected for slight light scattering by using a turbidity correction using software supplied with the HP8453 diode array spectrophotometers. An extinction coefficient for the bound FAD of the R194H mutants of lfALR was determined to be 11.4 mM^{-1} cm^{-1} at 456 nm, after release of flavin using 0.1% (w/v) SDS as described earlier (*39*). The comparable value for wild-type lfALR is 11.7 mM^{-1} cm^{-1} (*39*).

Sulfhydryl Oxidase Assays. Assays of ALR, monitored by the consumption of oxygen in a Clarke-type oxygen electrode, by reduction of cytochrome *c*, and by the oxidation of reduced human Mia40, were conducted as described previously (*38*, *39*).

Crystallization and Data Collection. Protein crystallization conditions were screened by hanging-drop vapor diffusion using Hampton Research crystal screening kits. Drops were generated at 25 °C by mixing 1 μL of the protein stock solution (8 mg/mL in 50 mM phosphate buffer, pH 7.5) with 1 μL of crystallization well solution. Promising conditions were refined to optimize crystal quality. The crystals used here (Figure S2, Supporting Information) were grown using a solution of 18% (w/v)PEG 8000, 210 mM zinc acetate dihydrate, and 100 mM sodium cacodylate, pH 6.5, that had been filtered through a 0.2 μm disposable filter unit (Nalgene). Crystals were dipped in a cryoprotectant mixture of the well solution containing 20% xylitol before flash-cooling in liquid nitrogen. Diffraction data were collected using in-house equipment (Rigaku RUH3R and R-AXIS IV). The crystal to detector distance was 100 mm, and the Cu radiation X-ray wavelength was 1.541 Å. Crystals were maintained at −180 °C, and data were collected for 15 min per 1° oscillation from a single crystal yielding a total of 180 diffraction images. The data were indexed, integrated, and scaled with the program HKL2000 (*47*).

Crystal Structure Solution and Refinement. The human sfALR structure was solved by molecular replacement using the coordinates for the rat sfALR dimer (PDB: 1OQC). Molecular replacement was carried out using the program MOLREP from the CCP4 suite of programs (*48*). Automated model building of human ALR employed ARP/wARP (*48*), and 30 cycles of refinements utilized REFMAC5 and COOT (*49*). Water molecules were placed during successive cycles of model building and refinement. The final human sfALR model (residues 81−205) had three subunits comprising of one covalent dimer and half of another covalent dimer whose dimer interface resided on a crystallographic symmetry axis. The N-terminus of each subunit was disordered, with the final model including residues 94−205 from each subunit. A final $2F_o - F_c$ electron density difference map (Figure S3, Supporting Information) confirmed the quality of the final model. The final $R_{working}$ and R_{free} values were 0.189 and 0.235, respectively.

In Silico Modeling. The R194H mutation of sfALR was modeled using the human sfALR structure using the program MODELER (*50*−*52*), optimized with variable target function and molecular dynamics (*51*), and further minimized using the CNS program (*53*, *54*). A total of 50 models were generated for the mutant R194H, and the structure with the lowest discrete optimized protein energy (DOPE) (*55*) was further minimized with CNS. DOPE values for the R194H model and the wild-type structure were comparable. The minimized model has rmsd of

0.013 Å and 1.74° pre- and post-CNS minimization, indicating good convergence. Solvent accessibilities for amino acid side chains and atoms were calculated using the NACCESS program (*56*).

Flavin Dissociation. lf- and sfALR were diluted to a concentration of 10 μM in 900 μL of 50 mM phosphate buffer, pH 7.5, 25 °C, containing 0.3 mM EDTA and 4.44 M guanidine hydrochloride. Flavin release was followed in an HP8453 diode array spectrophotometer by the decrease in absorbance at 496 nm.

FAD Association Rates. Apoproteins for sfALR wild type and the R194H mutant were prepared by incubating the sfALR holoprotein while bound to a Ni-NTA column (Invitrogen ProBond) with 10 mL of 50 mM phosphate buffer, pH 7.5, containing 6 M guanidine hydrochloride for 2 h followed by 10 mL of the same buffer without denaturant. The column was then immediately reequilibrated with denaturant and the treatment repeated three more times to ensure complete release of FAD. The column was developed using 5 mL aliquots of 50, 200, and 500 mM imidazole, and apo-ALR was desalted on a PD10 column equilibrated with 50 mM phosphate buffer, pH 7.5, containing 0.3 mM EDTA. Absorbance changes were monitored by stopped flow (SF-61 DX2 double mixing instrument; Hi-Tech) and analyzed using KinetAsyst 3 software.

Thermal Stability. The thermal stabilities of wild type and R194H mutants of lf- and sfALR were assessed using a JASCO 810 CD spectrophotometer. Far-UV (260−205 nm) CD spectra were collected at 2 °C increments every 10 min from 2 to 94 °C, in 1 mm path length cells using 10 μM ALR proteins. Mean residue ellipticities (deg cm^2 dmol^{-1}) were plotted as a function of temperature and used to calculate midpoint values.

NMR Data. The ^{1}H−^{15}N TROSY-HSQC NMR spectra were recorded at 25 °C using a Bruker AV600 MHz spectrometer equipped with a cryoprobe operating at 600.13 and 60.81 MHz for ^{1}H and ^{15}N, respectively. ^{15}N-Labeled wild-type and R194H sfALR proteins were expressed and purified as described above. NMR samples were prepared in 5 mm tubes containing 130 μM protein in 10 mM potassium phosphate buffer, pH 6.9, in 90% H_2O/10% D_2O. Acquisition parameters are listed in Supporting Information, and raw NMR data were processed using the NMRpipe program (*57*).

Partial Proteolysis. Wild type and R194H mutant sfALR (100 μM in 100 μL of 50 mM phosphate buffer, pH 7.5, 0.3 mM EDTA, 25 °C) were mixed with 1% (w/w) chymotrypsin. Aliquots (5 μL) were periodically removed, mixed with an equal volume of 2× nonreducing Laemmli buffer to arrest proteolysis, and then analyzed using 12% cross-linked SDS−PAGE gels.

Reduction of Intersubunit Disulfide Bonds with Glutathione. Wild-type and R194H sfALR (30 μM) were incubated in glass tubes with 10 mM GSH in 50 mM phosphate buffer and 0.3 mM EDTA, adjusted to pH 7.5. The tubes were sealed with serum caps, and the gas space was flushed with nitrogen through entry and exit needles. A narrow gauge needle could be threaded through the exit needle to withdraw 50 μL aliquots prior to quenching samples to a final concentration of 20 mM *N*-ethylmaleimide. Samples were then analyzed using 12% nonreducing SDS−PAGE gels and stained with Coomassie Brilliant Blue G-250. Bands for monomeric and dimeric ALR were quantitated using ImageJ (*58*).

RESULTS AND DISCUSSION

Location of R194 in Human ALR. Our previous studies of human ALR (*38*, *39*, *44*) have used a homology model for the short-form enzyme that was based on the rat sfALR dimer structure of Wu et al. (*5*). This model suggests that the R194 side chain of ALR would participate in several contacts, both with the ribose moiety of the FAD and with main chain atoms at the subunit interface (see later). This multiplicity of interactions suggested that an evaluation of the effect of the R194H mutation would be best undertaken with the cognate wild-type protein: human ALR. While we have yet to be successful in crystallizing human lfALR, with its 80-residue N-terminal extension (Figure 1A), crystals of the short-form enzyme were readily obtained (Figure S2, Supporting Information) and used for the structural determination described below. Although it is possible that some effects of the R194H mutant are unique to the long form of human ALR, none of the data presented here shows a selective impact between long and short versions of this flavoenzyme.

Table 1: Data Collection and Refinement Statistics of Human sfALR[a]

Data Collection	
space group	*C*2
unit cell dimensions	
a, *b*, *c* (Å)	112.719, 65.145, 63.767
α, *β*, *γ* (deg)	90.0, 89.973, 90.0
resolution (Å)	50.0−1.85 (1.92−1.85)[b]
completeness (%)	99.9 (100.0)
redundancy	3.6 (3.6)
$I/\sigma I$	36.54 (3.13)
R_{merge} linear[c]	0.044 (0.366)
Refinement	
resolution (Å)	63.76−1.85
R_{work}/R_{free}[d]	0.189/0.235
no. of atoms (non-hydrogen)	3429
mean *B* value	31.9
rmsd bond lengths (Å)	0.017
rmsd bond angles (deg)	1.94
Ramachandran plot	
most favored (%)	95.2
additionally and generously allowed region (%)	4.8

[a]Protein Data Bank accession code 3MBG. [b]Values in parentheses are for the highest resolution shell. [c]$R_{merge} = \sum|I_o - I_a|/\sum(I_a)$, where I_o is the observed intensity and I_a is the average intensity, the sums being taken over all symmetry-related reflections. [d]$R_{working} = \sum|F_o - F_c|/\sum(F_o)$, where F_o is the observed amplitude and F_c is the calculated amplitude. R_{free} is the equivalent of $R_{working}$, except it is calculated for a randomly chosen set of reflections that were omitted (5%) from the refinement process.

Crystal Structure of Human sfALR. Human sfALR crystallized rapidly without removal of the N-terminal His tag. The initial structure was solved using the rat sfALR (PDB: 1OQC) as a molecular replacement search model. The asymmetric unit consisted of three subunits: a disulfide-linked homodimer and half of an adjacent dimer. In all subunits, the first 27 N-terminal residues of the sfALR construct (Figure S1, Supporting Information, comprising 14 residues of the tag and linker, followed by 13 residues from the N-terminus of the cytokine form of ALR) were disordered. A summary of the data collection and refinement statistics for the crystal structure, encompassing residues D94-D205, is presented in Table 1. The overall fold of the covalent human sfALR dimer is shown in Figure 2. Figure S3, Supporting Information, shows a difference electron density map surrounding the bound FAD prosthetic group ($2F_o - F_c$) of this 1.85 Å structure. As would be expected from the level of protein sequence identity between rat and human short-form proteins

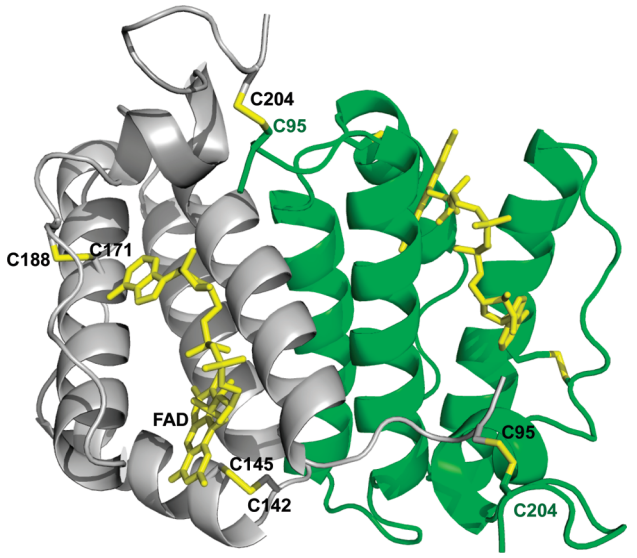

FIGURE 2: Overall chain fold of dimeric human sfALR. The two C95−C204 disulfides that join the gray and green subunits of the sfALR homodimer are shown in yellow, together with the redox-active proximal disulfide (C142−C145) and the structural disulfide (C171−C188) in the gray subunit. The FAD is depicted in yellow.

(85%), both dimers overlay very well (with an rmsd of 0.531 Å; Figure S4 in Supporting Information).

Figure 3A shows a stereoview of the human sfALR structure centered around R194. The residue is nearly coplanar with W195 suggestive of a cation−π interaction. One of the terminal guanidino amino groups of R194 forms H-bonds with two main chain carbonyl oxygen atoms: one from R194 itself and the other contributed by C95 of the other subunit. This particular cysteine residue participates in the two interchain disulfides (C95−C204 and its counterpart, C204−C95) that maintain ALR as a covalent head-to-tail dimer (Figure 2). A third H-bond links the δ-nitrogen of R194 to the 2′-OH of the ribose moiety of the bound FAD. This chain of interactions might reasonably be expected to link FAD binding with the conformational stabilization of the dimer interface in the vicinity of the interchain disulfide bridges (see later).

Despite the expectation that the R194H mutation would prove structurally conservative, numerous crystallization screening attempts with the mutant protein proved unsuccessful. Indeed, the mutation has an unexpectedly large effect on protein stability and flavin binding (see below), and this probably contributes to our inability to crystallize the protein over a wide range of conditions. Hence, for comparison with the native protein, we prepared an energy-minimized model of R194H (Figure 3B; see Experimental Procedures). This model introduced very small changes to the backbone (with a C_α rmsd of 0.244 Å) but generated significant perturbations in the region of residue 194. Here the imidazole ring of H194 is oriented at approximately right angles to the indole ring of W195. The model shows that H194 is now 3 Å from the 2′-OH of the FAD ribose in an orientation unfavorable for strong H-bond formation. While the importance of this potential H-bond in the R194H protein cannot be evaluated based on a modeled structure alone, the other two H-bonding interactions identified for the wild-type protein appear to be absent in the mutant (Figure 3B).

Comparison of UV−Vis Spectra of Wild Type and R194H Mutant. Since R194 makes H-bond contact with the 2′-OH ribose group of the FAD and participates in a network of

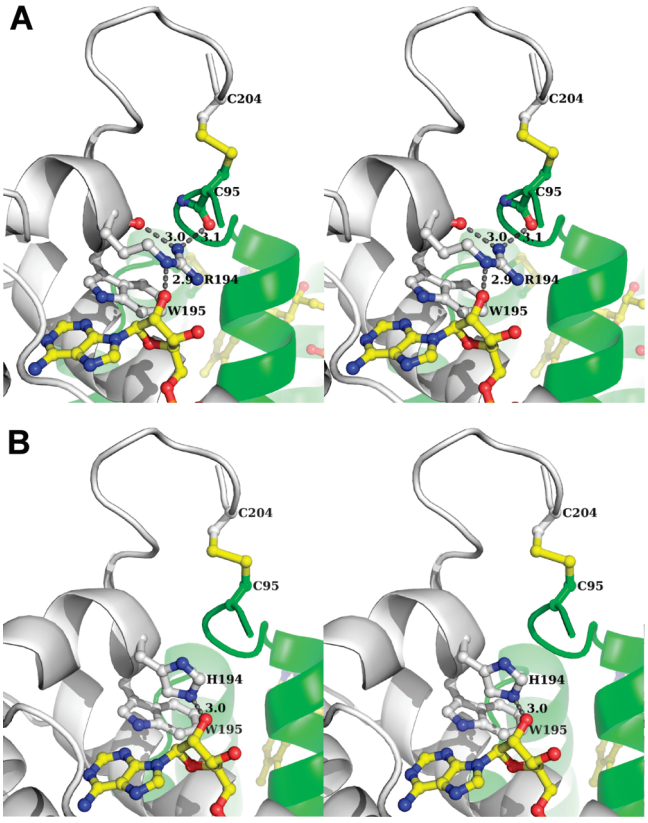

FIGURE 3: A stereoview surrounding R194 in human sfALR and a minimized model of the R194H mutant. Panel A: R194 forms H-bonds with the 2′-OH of the ribose moiety of FAD, with its own main chain peptide carbonyl, and with the main chain carbonyl oxygen contributed by C95 of the other (green) subunit. Panel B represents a minimized model (see Experimental Procedures) of the R194H sfALR mutant.

interactions around that region of the flavin prosthetic group, we examined whether the mutation produced significant differences in the spectrum of the bound isoalloxazine ring. First, it should be noted that there is approximately 20% less FAD bound to the R194H lfALR mutant than for the wild-type protein (for comparison, the main panel in Figure 4 normalizes these spectra at 280 nm). The inset shows that spectra of the bound flavin for wild-type and mutant lfALR are very similar (with comparable extinction coefficients for the bound flavin; see Experimental Procedures). Comparable measurements for sfALR show that about 15% less FAD is bound to the mutant protein; again, the normalized flavin spectra are comparable (Figure S5, Supporting Information).

Influence of R194H Mutation on the Enzymatic Activity of Human lf- and sfALR. Di Fonzo et al. made no direct assessment of the catalytic impact of the R194H mutant in human ALR or of the effects of the corresponding yeast Erv1p R182H mutant (*42*). Here we complement their studies using a range of in vitro assays of the long and short human ALR forms. Table 2 collects the steady-state catalytic parameters for these experiments (see Experimental Procedures). In all cases ALR concentrations of wild-type and mutant proteins were expressed in terms of flavin content (see Experimental Procedures) to normalize for the small differences in flavin loading mentioned above. Assays for lfALR utilized reduced Mia40 as the electron donor and either molecular oxygen or cytochrome *c* as oxidants (as described previously (*39*)). In terms of oxygen as an electron acceptor (Table 2, part B), small compensating changes in k_{cat}

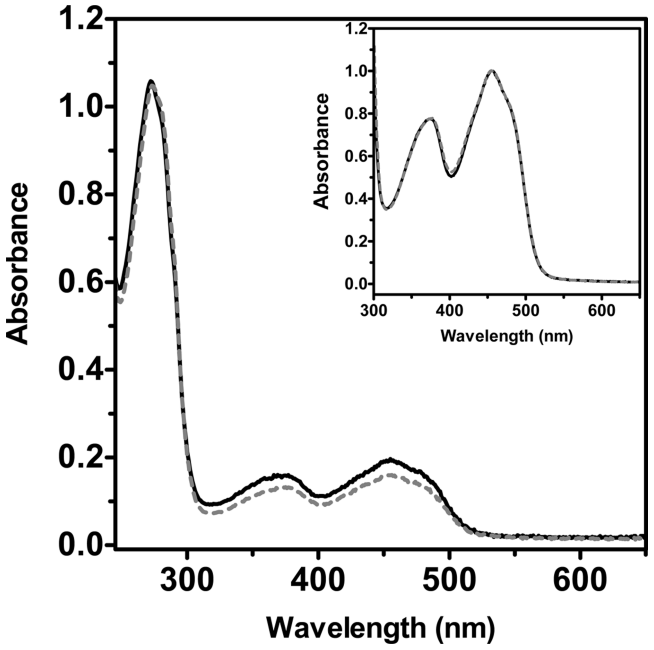

FIGURE 4: Comparison of UV−vis spectra of wild-type and R194 lfALR. Spectra were recorded in 50 mM phosphate buffer, pH 7.5, containing 0.3 mM EDTA and normalized either at 280 nm (main panel) or at 456 nm (inset). Spectra of wild type and the R194H mutant are shown by solid and dashed lines, respectively.

Table 2: Enzyme Activity of Wild Type and R194H Mutants of lf- and sfALR[a]

donor/acceptor	k_{cat} (min^{-1})	K_m (mM)	k_{cat}/K_m (M^{-1} s^{-1})
(A) DTT/O_2			
lfALR	61 ± 1.5	3 ± 0.3	330
lfALR R194H	72 ± 1	2.2 ± 0.1	550
sfALR	108 ± 7	1.6 ± 0.4	1100
sfALR R194H	73 ± 3	1.6 ± 0.25	760
(B) Mia40[b]/O_2			
lfALR	42 ± 8	0.068 ± 0.021	10200
lfALR R194H	24 ± 4	0.042 ± 0.014	9600
(C) Mia40[b]/Cyt *c*			
lfALR	48 ± 6	0.045 ± 0.012	17600
lfALR R194H	48 ± 9	0.039 ± 0.015	20700

[a]Three assay systems were used: (A) oxygen consumption in the oxygen electrode using DTT as a model substrate, (B) the oxygen-dependent reoxidation of reduced Mia40 followed discontinuously with DTNB, and (C) the reduction of cytochrome *c* followed continuously in the presence of reduced Mia40. [b]Kinetics determined with a shorter N-terminal linker for Mia40 than used previously (see Experimental Procedures (*39*)).

and K_m terms generate essentially the same catalytic efficiency of approximately 10^4 M^{-1} s^{-1}. For cytochrome *c* there is again no major difference between the k_{cat}/K_m terms (Table 2, part C). Using the model substrate DTT in the oxygen electrode, lfALR R194H mutant shows a catalytic efficiency some 1.7-fold higher than the native protein (Table 2, part A). In contrast, sfALR gives an approximate 30% decrease in k_{cat}/K_m values, again with minor changes in turnover and K_m parameters.

Overall, these data show that the kinetic impact of the R194H mutation in either human lf- or sfALR forms is minor. Di Fonzo et al. speculated that, in addition to the instability of lfALR induced by the R194H mutation, the mutant protein might be less efficient at transferring electrons to cytochrome *c* (*42*). Our data suggest that this latter possibility is unlikely to be a major factor in the R194H phenotype. The impaired assembly of cytochrome *c* oxidase observed earlier in vivo (*42*) probably reflects compromised folding of copper chaperones in the IMS deriving from a lowered concentration of active lfALR. We now document the impact of R194H on the stability and flavin binding of human ALR.

Table 3: Melting Temperature of Wild Type and R194H Mutant of lf- and sfALR[a]

construct	T_m (°C)
lfALR	86
lfALR R194H	75
sfALR	86
sfALR R194H	78

[a]Measured by circular dichroism at 222 nm in 50 mM phosphate buffer, pH 7.5, containing 0.3 mM EDTA (see Experimental Procedures).

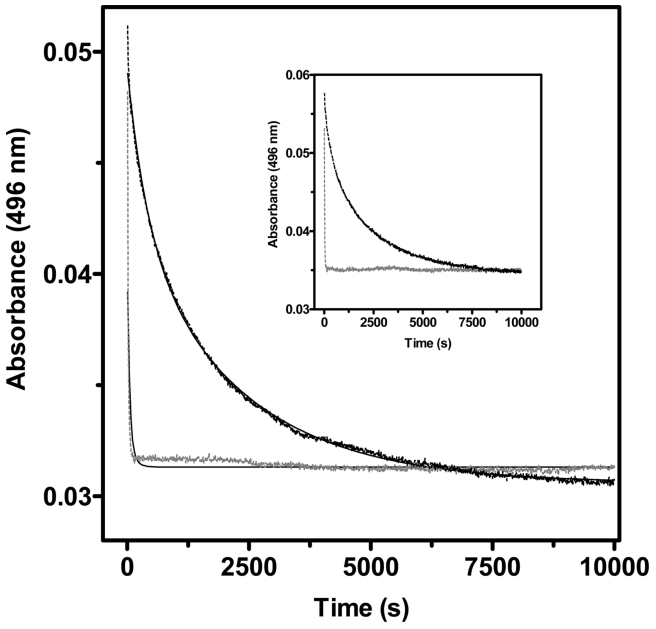

FIGURE 5: Comparison of rate of flavin release from wild type and R194H mutants of ALR. The main panel monitors the absorbance at 496 nm after the addition of 4.44 M guanidine hydrochloride in 50 mM phosphate buffer, pH 7.5, 25 °C (black line). The gray line represents the rapid release of FAD from the R194H lfALR mutant. The inset presents the corresponding experiments with the short form of ALR.

Thermal Stability. Human sfALR shows considerable thermal stability with CD parameters only changing at temperatures above 70 °C (*59*). Thermal denaturation experiments following wild type and mutant lf- and sfALR in the CD show that the mutants have a T_m about 10 °C lower than wild-type proteins (Table 3; see Experimental Procedures).

Flavin Dissociation. A striking demonstration of the impact of the R194H mutation is provided in Figure 5. Both wild type and the R194H mutants of lf- and sfALR were challenged with 4.4 M guanidine hydrochloride, and the release of FAD was evaluated by the decrease in absorbance at 496 nm. For wild-type lfALR, the half-time required for release of FAD from the wild-type protein is 900 s compared to about 20 s for the mutant. The same relative susceptibility is observed for sfALR (inset, Figure 5), again suggesting that the impact of the R194H mutant can be appropriately assessed in the context of the shorter ALR construct.

FAD Binding to Wild-Type and R194H ALR. Since all of the studies mentioned above show comparable effects of the

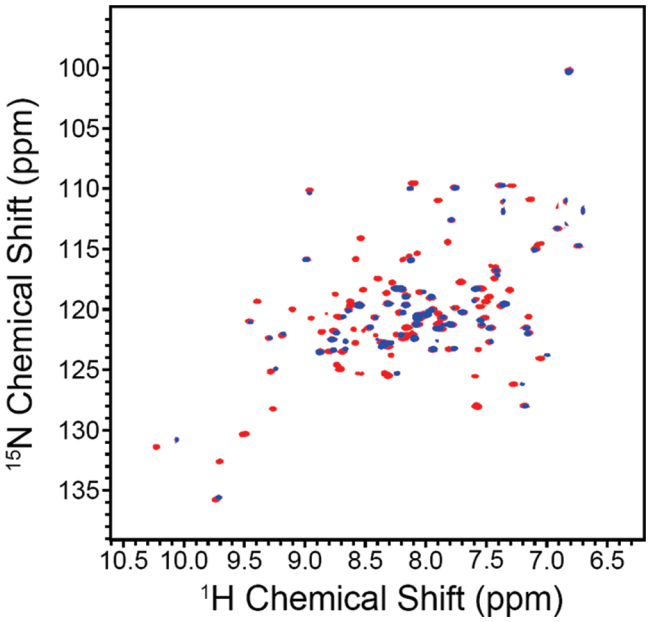

FIGURE 6: 2D ^{1}H−^{15}N TROSY-HSQC spectra of wild type and R194H mutant of sfALR. Wild type (red) and R194H (blue) spectra were acquired in 10 mM phosphate buffer, pH 6.9 at 25 °C (see Experimental Procedures).

R194H mutant on the long and short forms of ALR, we have utilized the more readily accessible sfALR in the following sections. When FAD binding to apo-sfALR was evaluated in the stopped-flow spectrophotometer by following the absorbance increase at 490 nm, both wild type and mutant behaved comparably (with closely superimposable kinetics; Figure S6 in Supporting Information).

In complementary experiments, we examined the return of ALR activity using DTT as a substrate in the oxygen electrode following the addition of FAD to the apo forms of lf- and sfALR. In both mutant and wild-type instances the oxygen traces observed were the same as those observed with the corresponding concentration of holo-sfALR (data not shown). While equilibration of the oxygen electrode requires several seconds, these results suggest that flavin binding and activity return for wild-type and mutant ALR are comparably rapid. Hence the weaker FAD binding encountered with the mutant seems to largely reflect the dissociation rate constant from the holoprotein.

Comparison between Wild Type and R194H Mutants by TROSY-HSQC NMR. Figure 6 presents an overlay of 2D NMR spectra of ^{15}N-labeled wild-type (red) and R194H sfALR (blue) proteins acquired under identical conditions (see Experimental Procedures). The dispersion of chemical shifts shows that both proteins are well ordered, although the mutant shows considerably fewer resonances over the range depicted in Figure 6 (approximately 40% less). These absences are consistent with enhanced selective flexibility of the R194H mutant compared to the native protein.

The R194H Mutant of Human ALR Acquires Protease Sensitivity. One consequence of the increased protein mobility noted above may be a corresponding increase in susceptibility to intracellular proteases. Figure 7 shows that wild-type sfALR was resistant to incubation with 1% (w/w) chymotrypsin over 2 h at 25 °C in potassium phosphate buffer, pH 7.5. This stability extended to 5 h without significant change in the appearance of bands in these nonreducing gels (data not shown). In contrast, the mutant protein showed significant proteolysis after 1 min (with

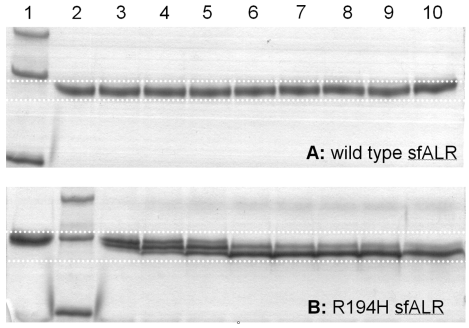

FIGURE 7: The R194H mutant of sfALR gains sensitivity to partial proteolysis using chymotrypsin. Nonreducing SDS−PAGE gels were run with protein standards (35, 25, and 15 kDa from the top of panel A, lane 1; and panel B, lane 2). R194H (lane 1, panel B) reproducibly runs slightly slower than wild-type protein (lane 2, panel A) on SDS−PAGE. Proteins were treated with 1% (w/w) chymotrypsin in 50 mM phosphate buffer, pH 7.5, 25 °C, containing 0.3 mM EDTA, and samples were quenched in nonreducing Laemmli buffer (for panel A, lanes 2−10 were quenched 0, 1, 3, 5, 10, 15, 30, 60, and 120 min after protease treatment of sfALR). For the mutant in panel B, lane 1 is at time zero, lane 2 is the protein ladder, and lanes 3−10 reflect the same time intervals as in panel A. For clarity, the dotted lines on the gels define the limits of band migration.

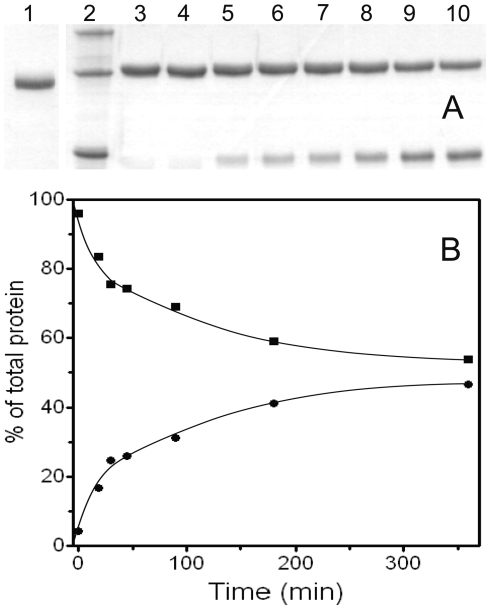

FIGURE 8: The R194H sfALR mutant is sensitive to reduction of intersubunit disulfide bonds. Panel A: After 6 h of anaerobic incubation of 30 μM wild-type sfALR with 10 mM GSH followed by quenching with 20 mM NEM (see Experimental Procedures), the protein runs exclusively as a dimer on nonreducing SDS−PAGE (lane 1). Lane 2 represents molecular mass markers (from the top: 35, 25, and 15 kDa). Lane 3 shows the R194H mutation in the absence of GSH, and lanes 4−10 are 0, 18, 30, 45, 90, 180, and 360 min after the addition of 10 mM GSH. Panel B: Time dependence of the integrated intensities of the stained bands (square and circles represent dimer and monomer bands, respectively; see Experimental Procedures).

the appearance of a band running slightly faster than the original; Figure 7). Further incubation with chymotrypsin generated additional truncation of R194H sfALR and disappearance of the band corresponding to the original protein after 5 min.

The R194H Mutant Is Susceptible to Reduction by Glutathione. The sensitivity of the mutant protein to limited proteolysis using chymotrypsin, and the pronounced flexibility apparent from the TROSY-HSQC experiments, suggests that the region surrounding R194 has a significant effect on both local

and global structure of human ALR. Hence we tested whether the mutation might destabilize the unusual interchain disulfides between the N-terminus of one subunit and the C-terminus of the other (Figure 2). Specifically, we investigated whether these cross-links in the mutant protein are prone to reduction by realistic cellular concentrations of GSH. The reductive monomerization of wild-type sfALR is very slow using 10 mM GSH at 25 °C; under anaerobic conditions no monomer was evident over 6 h (Figure 8). Samples were analyzed in this experiment by nonreducing SDS−PAGE after quenching with excess NEM (see Experimental Procedures). Reductive incubations were performed anaerobically because, while GSH is an extremely poor substrate of ALR (*38*, *39*), GSSG might slowly accumulate over prolonged aerobic incubation using micromolar concentrations of the oxidase. In contrast to wild-type sfALR, reduction of the C95−C204 disulfide bonds is clearly evident after 18 min incubation with the mutant protein (Figure 8A, lane 5). Figure 8B shows a time course of the reduction of these interchain disulfide bridges in the R194H sfALR mutant. Finally, the sensitivity of the apoprotein forms of wild-type and mutant sfALR to the same reductive conditions was investigated (see Experimental Procedures). The wild-type apoprotein again remains resistant to 10 mM GSH (with 90% dimer retained after 5 h), compared to only 16% with the mutant protein (data not shown).

The sluggish reduction of the wild-type protein by GSH is of interest because the interchain C95−204 disulfides appear significantly solvent-accessible in the holoprotein (the side chains of C95 and C204 are 45% and 8% accessible, respectively; see Experimental Procedures (*56*)). Nevertheless, in vitro these disulfides in the wild-type protein remain intact for hours under anaerobic conditions in the presence of 10 mM GSH. While the unusual topology of these disulfides, securing the N- and C-termini within a homodimer, is suggestive of functional importance, their role is currently obscure. While such disulfides are found in many eukaryotic ALR analogues (from *Aspergillus* to humans), they are absent in both budding and nonbudding yeast.

Conclusions. These data show the unexpectedly severe impact of R194H on the conformational stability of both long and short forms of human ALR. They complement the studies of Comi and co-workers (*42*) and provide strong in vitro corroboration of their suggestions that the R194H mutant is significantly destabilizing. Our studies provide a molecular rationale for this marked loss of stability, evident by an increased rate of dissociation of FAD from the mutant ALR, an enhanced susceptibility to partial proteolysis and to reduction of the interchain disulfide bonds, and a major loss of order as measured by 2D NMR. The unanticipated severity of these effects points to a strong influence of the interchain disulfide bonds, the neighboring amino acid residues, and the bound FAD on the stability of dimeric ALR. In contrast, the catalytic activity of the mutant protein is not compromised by the replacement of R194 by a histidine residue.

ACKNOWLEDGMENT

We thank Mr. Shangjin Sun and Drs. Steve Bai and Tatyana Polenova for help with the NMR measurements and analysis. Dr. Vamsi Kodali is acknowledged for helpful comments.

SUPPORTING INFORMATION AVAILABLE

Table S1 and Figures S1−S6 providing data, sequences, and analysis for human sfALR and its R194H mutant. This material is available free of charge via the Internet at http://pubs.acs.org.

REFERENCES

1. Lee, J., Hofhaus, G., and Lisowsky, T. (2000) Erv1p from *Saccharomyces cerevisiae* is a FAD-linked sulfhydryl oxidase. *FEBS Lett. 477* (1−2), 62–66.
2. Lisowsky, T. (1994) ERV1 is involved in the cell-division cycle and the maintenance of mitochondrial genomes in *Saccharomyces cerevisiae*. *Curr. Genet. 26*, 15–20.
3. Fass, D. (2008) The Erv family of sulfhydryl oxidases. *Biochim. Biophys. Acta 1783*, 557–566.
4. Gross, E., Sevier, C. S., Vala, A., Kaiser, C. A., and Fass, D. (2002) A new FAD-binding fold and intersubunit disulfide shuttle in the thiol oxidase Erv2p. *Nat. Struct. Biol. 9*, 61–67.
5. Wu, C. K., Dailey, T. A., Dailey, H. A., Wang, B. C., and Rose, J. P. (2003) The crystal structure of augmenter of liver regeneration: a mammalian FAD-dependent sulfhydryl oxidase. *Protein Sci. 12*, 1109–1118.
6. Gross, E., Kastner, D. B., Kaiser, C. A., and Fass, D. (2004) Structure of Ero1p, source of disulfide bonds for oxidative protein folding in the cell. *Cell 117*, 601–610.
7. Hoober, K. L., Glynn, N. M., Burnside, J., Coppock, D. L., and Thorpe, C. (1999) Homology between egg white sulfhydryl oxidase and quiescin Q6 defines a new class of flavin-linked sulfhydryl oxidases. *J. Biol. Chem. 274*, 31759–31762.
8. Alon, A., Heckler, E., Thorpe, C., and Fass, D. (2010) QSOX contains a pseudo-dimer of functional and degenerate sulfhydryl oxidase domains. *FEBS Lett. 584*, 1521–1525.
9. Thorpe, C., and Coppock, D. L. (2007) Generating disulfides in multicellular organisms: emerging roles for a new flavoprotein family. *J. Biol. Chem. 282*, 13929–13933.
10. Heckler, E. J., Rancy, P. C., Kodali, V. K., and Thorpe, C. (2008) Generating disulfides with the quiescin-sulfhydryl oxidases. *Biochim. Biophys. Acta 1783*, 567–577.
11. Chen, X., Li, Y., Wei, K., Li, L., Liu, W., Zhu, Y., Qiu, Z., and He, F. (2003) The potentiation role of hepatopoietin on activator protein-1 is dependent on its sulfhydryl oxidase activity. *J. Biol. Chem. 278*, 49022–49030.
12. Pawlowski, R., and Jura, J. (2006) ALR and liver regeneration. *Mol. Cell. Biochem. 288*, 159–169.
13. Lisowsky, T., Lee, J. E., Polimeno, L., Francavilla, A., and Hofhaus, G. (2001) Mammalian augmenter of liver regeneration protein is a sulfhydryl oxidase. *Dig. Liver Dis. 33*, 173–180.
14. Li, Y., Wei, K., Lu, C., Li, M., Xing, G., Wei, H., Wang, Q., Chen, J., Wu, C., Chen, H., Yang, S., and He, F. (2002) Identification of hepatopoietin dimerization, its interacting regions and alternative splicing of its transcription. *Eur. J. Biochem. 269*, 3888–3893.
15. Gatzidou, E., Kouraklis, G., and Theocharis, S. (2006) Insights on augmenter of liver regeneration cloning and function. *World J. Gastroenterol. 12*, 4951–4958.
16. Polimeno, L., Lisowsky, T., and Francavilla, A. (1999) From yeast to man—from mitochondria to liver regeneration: a new essential gene family. *Ital. J. Gastroenterol. Hepatol. 31*, 494–500.
17. LaBrecque, D. R., and Pesch, L. A. (1975) Preparation and partial characterization of hepatic regenerative stimulator substance (SS) from rat liver. *J. Physiol. 248*, 273–284.
18. Hagiya, M., Francavilla, A., Polimeno, L., Ihara, I., Sakai, H., Seki, T., Shimonishi, M., Porter, K. A., and Starzl, T. E. (1994) Cloning and sequence analysis of the rat augmenter of liver regeneration (ALR) gene: expression of biologically active recombinant ALR and demonstration of tissue distribution. *Proc. Natl. Acad. Sci. U.S.A. 91*, 8142–8146.
19. Wang, G., Yang, X., Zhang, Y., Wang, Q., Chen, H., Wei, H., Xing, G., Xie, L., Hu, Z., Zhang, C., Fang, D., Wu, C., and He, F. (1999) Identification and characterization of receptor for mammalian hepatopoietin that is homologous to yeast ERV1. *J. Biol. Chem. 274*, 11469–11472.
20. Gandhi, C. R., Murase, N., and Starzl, T. E. (2010) Cholera toxin-sensitive GTP-binding protein-coupled activation of augmenter of liver regeneration (ALR) receptor and its function in rat kupffer cells. *J. Cell. Physiol. 222*, 365–373.
21. Li, Y., Li, M., Xing, G., Hu, Z., Wang, Q., Dong, C., Wei, H., Fan, G., Chen, J., Yang, X., Zhao, S., Chen, H., Guan, K., Wu, C., Zhang, C., and He, F. (2000) Stimulation of the mitogen-activated protein kinase cascade and tyrosine phosphorylation of the epidermal growth factor receptor by hepatopoietin. *J. Biol. Chem. 275*, 37443–37447.
22. Liao, X. H., Zhang, L., Liu, Q., Sun, H., Peng, C. M., and Guo, H. (2010) Augmenter of liver regeneration protects kidneys from ischaemia/reperfusion injury in rats, Nephrol. Dial. Transplant. (EPUB ahead of print).
23. Shen, L., Hu, J., Lu, H., Wu, M., Qin, W., Wan, D., Li, Y. Y., and Gu, J. (2003) The apoptosis-associated protein BNIPL interacts with two

cell proliferation-related proteins, MIF and GFER. *FEBS Lett. 540*, 86–90.
24. Boyd, J. M., Malstrom, S., Subramanian, T., Venkatesh, L. K., Schaeper, U., Elangovan, B., D'Sa-Eipper, C., and Chinnadurai, G. (1994) Adenovirus E1B 19 kDa and Bcl-2 proteins interact with a common set of cellular proteins. *Cell 79*, 341–351.
25. Lu, C., Li, Y., Zhao, Y., Xing, G., Tang, F., Wang, Q., Sun, Y., Wei, H., Yang, X., Wu, C., Chen, J., Guan, K. L., Zhang, C., Chen, H., and He, F. (2002) Intracrine hepatopoietin potentiates AP-1 activity through JAB1 independent of MAPK pathway. *FASEB J. 16*, 90–92.
26. Mesecke, N., Terziyska, N., Kozany, C., Baumann, F., Neupert, W., Hell, K., and Herrmann, J. M. (2005) A disulfide relay system in the intermembrane space of mitochondria that mediates protein import. *Cell 121*, 1059–1069.
27. Terziyska, N., Grumbt, B., Bien, M., Neupert, W., Herrmann, J. M., and Hell, K. (2007) The sulfhydryl oxidase Erv1 is a substrate of the Mia40-dependent protein translocation pathway. *FEBS Lett. 581*, 1098–1102.
28. Gabriel, K., Milenkovic, D., Chacinska, A., Muller, J., Guiard, B., Pfanner, N., and Meisinger, C. (2007) Novel mitochondrial intermembrane space proteins as substrates of the MIA import pathway. *J. Mol. Biol. 365*, 612–620.
29. Hell, K. (2008) The Erv1-Mia40 disulfide relay system in the intermembrane space of mitochondria. *Biochim. Biophys. Acta 1783*, 601–609.
30. Herrmann, J. M., and Kohl, R. (2007) Catch me if you can! Oxidative protein trapping in the intermembrane space of mitochondria. *J. Cell Biol. 176*, 559–563.
31. Beverly, K. N., Sawaya, M. R., Schmid, E., and Koehler, C. M. (2008) The Tim8-Tim13 complex has multiple substrate binding sites and binds cooperatively to Tim23. *J. Mol. Biol. 382*, 1144–1156.
32. Stojanovski, D., Milenkovic, D., Muller, J. M., Gabriel, K., Schulze-Specking, A., Baker, M. J., Ryan, M. T., Guiard, B., Pfanner, N., and Chacinska, A. (2008) Mitochondrial protein import: precursor oxidation in a ternary complex with disulfide carrier and sulfhydryl oxidase. *J. Cell Biol. 183*, 195–202.
33. Tokatlidis, K. (2005) A disulfide relay system in mitochondria. *Cell 121*, 965–967.
34. Reddehase, S., Grumbt, B., Neupert, W., and Hell, K. (2009) The disulfide relay system of mitochondria is required for the biogenesis of mitochondrial Ccs1 and Sod1. *J. Mol. Biol. 385*, 331–338.
35. Kawamata, H., and Manfredi, G. (2008) Different regulation of wild-type and mutant Cu,Zn superoxide dismutase localization in mammalian mitochondria. *Hum. Mol. Genet. 17*, 3303–3317.
36. Lange, H., Lisowsky, T., Gerber, J., Muhlenhoff, U., Kispal, G., and Lill, R. (2001) An essential function of the mitochondrial sulfhydryl oxidase Erv1p/ALR in the maturation of cytosolic Fe/S proteins. *EMBO Rep. 2*, 715–720.
37. Allen, S., Balabanidou, V., Sideris, D. P., Lisowsky, T., and Tokatlidis, K. (2005) Erv1 mediates the Mia40-dependent protein import pathway and provides a functional link to the respiratory chain by shuttling electrons to cytochrome *c*. *J. Mol. Biol. 353*, 937–944.
38. Farrell, S. R., and Thorpe, C. (2005) Augmenter of liver regeneration: a flavin dependent sulfhydryl oxidase with cytochrome *c* reductase activity. *Biochemistry 44*, 1532–1541.
39. Daithankar, V. N., Farrell, S. R., and Thorpe, C. (2009) Augmenter of liver regeneration: substrate specificity of a flavin-dependent oxidoreductase from the mitochondrial intermembrane space. *Biochemistry 48*, 4828–4837.
40. Bihlmaier, K., Mesecke, N., Terziyska, N., Bien, M., Hell, K., and Herrmann, J. M. (2007) The disulfide relay system of mitochondria is connected to the respiratory chain. *J. Cell Biol. 179*, 389–395.
41. Dabir, D. V., Leverich, E. P., Kim, S. K., Tsai, F. D., Hirasawa, M., Knaff, D. B., and Koehler, C. M. (2007) A role for cytochrome *c* and cytochrome *c* peroxidase in electron shuttling from Erv1. *EMBO J. 26*, 4801–4811.
42. Di Fonzo, A., Ronchi, D., Lodi, T., Fassone, E., Tigano, M., Lamperti, C., Corti, S., Bordoni, A., Fortunato, F., Nizzardo, M., Napoli, L., Donadoni, C., Salani, S., Saladino, F., Moggio, M., Bresolin, N., Ferrero, I., and Comi, G. P. (2009) The mitochondrial disulfide relay system protein GFER is mutated in autosomal-recessive myopathy with cataract and combined respiratory-chain deficiency. *Am. J. Hum. Genet. 84*, 594–604.
43. Cobine, P. A., Pierrel, F., and Winge, D. R. (2006) Copper trafficking to the mitochondrion and assembly of copper metalloenzymes. *Biochim. Biophys. Acta 1763*, 759–772.
44. Kay, C. W. M., Elsasser, C., Bittl, R., Farrell, S. R., and Thorpe, C. (2006) Determination of the distance between the two neutral flavin radicals in augmenter of liver regeneration by pulsed ELDOR. *J. Am. Chem. Soc. 128*, 76–77.
45. Ang, S. K., and Lu, H. (2009) Deciphering structural and functional roles of individual disulfide bonds of the mitochondrial sulfhydryl oxidase Erv1p. *J. Biol. Chem. 284*, 28754–28761.
46. Marley, J., Lu, M., and Bracken, C. (2001) A method for efficient isotopic labeling of recombinant proteins. *J. Biomol. NMR 20*, 71–75.
47. Otwinowski, Z., and Minor, W. (1997) Processing of X-ray diffraction data collected in oscillation mode. *Macromol. Cryst., Part A 276*, 307–326.
48. Bailey, S. (1994) The Ccp4 suite—programs for protein crystallography. *Acta Crystallogr. D 50*, 760–763.
49. Emsley, P., and Cowtan, K. (2004) Coot: model-building tools for molecular graphics. *Acta Crystallogr. D 60*, 2126–2132.
50. Pieper, U., Eswar, N., Webb, B. M., Eramian, D., Kelly, L., Barkan, D. T., Carter, H., Mankoo, P., Karchin, R., Marti-Renom, M. A., Davis, F. P., and Sali, A. (2009) MODBASE, a database of annotated comparative protein structure models and associated resources. *Nucleic Acids Res. 37*, D347–D354.
51. Sali, A., and Blundell, T. L. (1993) Comparative protein modelling by satisfaction of spatial restraints. *J. Mol. Biol. 234*, 779–815.
52. Eswar, N., Webb, B., Marti-Renom, M., Madhusudhan, M., Eramian, D., Shen, M.-y., Pieper, U., and Sali, A. (2007) Comparative protein structure modeling using MODELLER, in Current Protocols in Protein Science, pp 1−31, Wiley, New York.
53. Brunger, A. T. (2007) Version 1.2 of the crystallography and NMR system. *Nat. Protoc. 2*, 2728–2733.
54. Brunger, A. T., Adams, P. D., Clore, G. M., DeLano, W. L., Gros, P., Grosse-Kunstleve, R. W., Jiang, J. S., Kuszewski, J., Nilges, M., Pannu, N. S., Read, R. J., Rice, L. M., Simonson, T., and Warren, G. L. (1998) Crystallography & NMR system: a new software suite for macromolecular structure determination. *Acta Crystallogr., Sect. D: Biol. Crystallogr. 54*, 905–921.
55. Shen, M. Y., and Sali, A. (2006) Statistical potential for assessment and prediction of protein structures. *Protein Sci. 15*, 2507–2524.
56. Hubbard, S., and Thornton, J. (1993) NACCESS, computer program, Department of Biochemistry and Molecular Biology, University College, London.
57. Delaglio, F., Grzesiek, S., Vuister, G. W., Zhu, G., Pfeifer, J., and Bax, A. (1995) NMRPipe: a multidimensional spectral processing system based on UNIX pipes. *J. Biomol. NMR 6*, 277–293.
58. Abramoff, M., Magelhaes, P., and Ram, S. J. (2004) Image processing with ImageJ. *Biophotonics Int. 11*, 36–42.
59. Yang, Z. C., Yang, L., Zhang, Y. X., Yu, H. F., and An, W. (2007) Effect of heat and pH denaturation on the structure and conformation of recombinant human hepatic stimulator substance. *Protein J. 26*, 303–313.